UNIVERSITY OF SÃO PAULO
SÃO CARLOS SCHOOL OF ENGINEERING

Gabriel José Negrelli Gomes

Development of Software for Parameter Estimation of Wind Power Plant Equivalent

São Carlos

2019

Gabriel José Negrelli Gomes

Development of Software for Parameter Estimation of Wind Power Plant Equivalent

Qualification submitted to the São Carlos School of Engineering of the University of São Paulo in partial fulfillment of the requirements for the degree of Master of Science in Electrical Engineering.

Area: Electrical Power Systems

Supervisor: Prof. Dr. Elmer Pablo Tito Cari

São Carlos

2019

ABSTRACT

GOMES, G. J. N.   **Development of Software for Parameter Estimation of Wind Power Plant Equivalent**. 2019. 49p. Dissertation (Masters) - São Carlos School of Engineering, University of São Paulo, São Carlos, 2019.

This project proposes the development of a software for identification of wind power plant equivalent models. To achieve this goal, a generic model well-known in the literature, capable of representing wind power plants during transients, was chosen. The method applied to identify the model is composed of two optimization algorithms. At the begining of the process, an heuristic approach based on Mean-Variance Mapping Optimization is used in order to reduce the parameter's search region around a possible solution. Afterward, a non-linear algorithm based on Trajectory Sensitivity is used to determine the local minimum and estimate the parameters. The method validation will be made using data from simulated systems. Also, a guided user interface will be developed in Python for this application, aiding new users.

Keywords: Wind power plants. Parameter estimation. MVMO. Trajectory sensitivity. Python.

RESUMO

GOMES, G. J. N. **Desenvolvimento de Software para Estimação de Parâmetros de Equivalentes Eólicos**. 2019. 49p. Dissertation (Masters) - São Carlos School of Engineering, University of São Paulo, São Carlos, 2019.

O presente trabalho propõe o desenvolvimento de um *software* para identificação de um modelo equivalente de parques eólicos. Para este objetivo foi escolhido um modelo genérico da literatura capaz de representar de forma adequada o comportamento da planta eólica durante transitórios. O método utilizado para a identificação do modelo é constituído por dois algoritmos de otimização. Primeiramente, é empregada uma abordagem heurística, baseada em Otimização por Mapeamento de Média-Variância, a fim de reduzir a região de busca dos parâmetros em torno de uma possível solução. Em seguida, utiliza-se um algoritmo não-linear, baseado no Método de Sensibilidade de Trajetória, para determinar o mínimo local e estimar os valores dos parâmetros com mais precisão. A validação do método será feita utilizando medidas de sistemas simulados. Com o intuito de facilitar a experiência do usuário com o programa, será desenvolvida uma interface gráfica amigável em Python.

Palavras-chave: Plantas eólicas. Estimação de parâmetros. MVMO. Sensibilidade de trajetória. Python.

LIST OF FIGURES

LIST OF TABLES

LIST OF ABBREVIATIONS AND ACRONYMS

ABEEólica   Brazilian Wind Energy Association

ANEEL   Brazilian Electricity Regulatory Agency

DFIG   Doubly Fed Induction Generator

EESG   Electrical Excited Synchronous Generator

EU   European Union

GUI   Graphical User Interface

IEEE   Institute of Electrical and Electronics Engineers

MVMO   Mean-Variance Mapping Optimization

PMSG   Permanent Magnet Synchronous Generator

PROINFA   Program of Incentive to Alternative Electric Energy Sources

SCIG   Squirrel Cage Induction Generator

TSM   Trajectory Sensitivity Method

US   United States of America

UK   United Kingdom

WECC   Western Electricity Coordinating Council

WRIG   Wound Rotor Induction Generator

WTG   Wind Turbine Generator

CONTENTS

1 INTRODUCTION

During the last decade, the world has seen an increase in participation of renewable sources in power generation, leaded mainly by wind and solar energy. These green technologies provide an alternative to sources based on fossil fuel, lowering pollution levels and reducing greenhouse gas emissions. On the other hand, the power output from these sources rely on weather conditions and cannot be fully controlled.

This increase is seen worldwide, as part of policies to reduce the human impact on climate and the environment. This 'renewable wave' is leaded mainly by European countries, specially in the European Union (EU), United States (US) and China. In particular, EU has set in 2010 a strategy plan to reduce its greenhouse emissions by at least 20% compared to 1990 levels and increase the share of renewable sources to at least 20% by 2020 (European Commission, 2010).

Brazil does not lag far behind EU regarding renewable sources policies. In 2002, the country passed a bill that, among other actions, creates the Program of Incentive to Alternative Electric Energy Sources (PROINFA). This program aims to increase the share of wind, solar, small hydro and biomass energy production. The final goal is to have these energy sources corresponding to 10% of Brazil's annual energy consumption by 2024 (Federative Republic of Brazil, 2002).

1.1 Wind Energy

Those policies promoted the increase of wind energy participation, reaching a scenario where it is one of the main energy sources of some countries, such as Denmark and Ireland. In the EU, wind energy alone generated 362 TWh in 2018, covering 14% of the electricity demand, a share 2% higher than 2017, with wind turbines installed both onshore (within the countries) and offshore (in the ocean). Among the EU countries, Denmark leads in this sector, with 41% of its demand supplied by wind power plants, followed by Ireland (28%), Portugal (24%) and Germany (21%). The total installed capacity across the 28 EU countries is 178.8 GW, with Germany in first position, with a total installed capacity of 59.3 GW, followed by Spain and the United Kingdom (UK), with 23.5 and 21.0 GW installed, respectively (Wind Europe, 2019). Figure 1 displays the detailed percentage of electricity demand covered by wind in the EU.

In Brazil, wind energy contributed to the electricity matrix with 42.4 TWh during 2017, resulting in a participation share of 7.2%. For comparison, Itaipu, the largest power plant in Brazil, has produced 96.4 TWh during the same period. But, while other sources, such as hydro and coal, had its share lowered, wind energy had the highest increase among

Figure 1: Share of electricity demand in the EU covered by wind energy during 2018
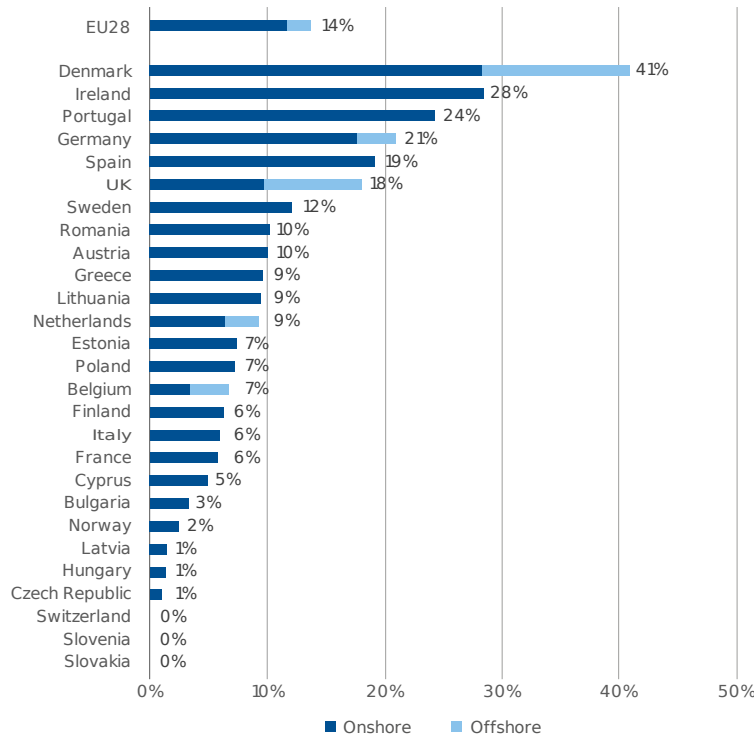
Source: Wind Europe, 2019

sources comparing to 2016, increasing its contribution by 26.5% (EPE, 2018).

Regarding the installed capacity, wind power plants appear in 2nd place, with 14.7 GW installed, only behind hydro power plants (ABEEOLICA, 2018), as shown in Figure 2. However, there is still plenty of energy yield for this source to be explored. In (AMARANTE et al., 2001) is shown that Brazil has potential to generate 272.2 TWh per year, with an installed capacity of 143.5 GW. The Northeast Region has the higher potential, with an annual energy yield of 144.3 TWh and potential to host up to 75.0 GW . Also, the wind regime in the Northeast Region is complimentary to the water regime of the main river responsible to power generation in the region, as presented by Figure 3. This characteristic would help controlling reservoir water level during dry season, an important resource not only for power generation, but also irrigation of crops and water supply (ANEEL, 2005).

Therefore, it is expected that wind energy will increase its participation in electricity generation in the next years. However, some aspects of the wind energy must be considered prior to the implementation on large scale of wind power plants.

The main difficulties are due to the nature of the energy source and the generator's characteristics. The wind regime is not constant and evenly distributed across the country, depending on the region's geography and vegetation. This results in a energy source that

Figure 2: Electricity generation in Brazil by source
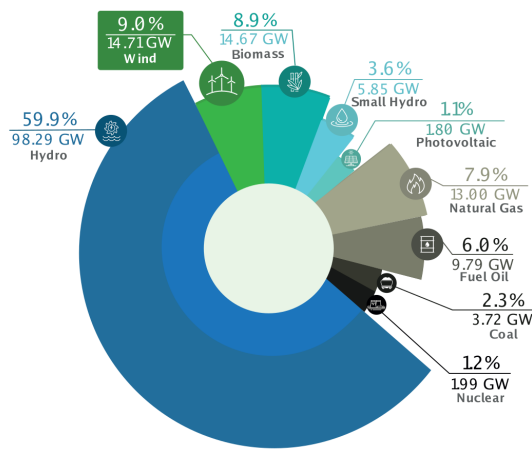
Source: ABEEólica, 2018

is not entirely reliable and concentrated on a certain area. Wind turbine generators usually have their rotor decoupled from the grid via frequency converter, leading to their low inertia. Thus, the system may experience stability problems during transients due to the high penetration of these machines (XIONG et al., 2019).

In order to maintain the electrical power system reliable, studies simulating various conditions must be performed beforehand, so the operators can be prepared for every occasion. These studies require mathematical models capable of adequately simulate the behaviour of every component on the grid.

Figure 3: Wind and water regime in the Brazilian Northeast Region
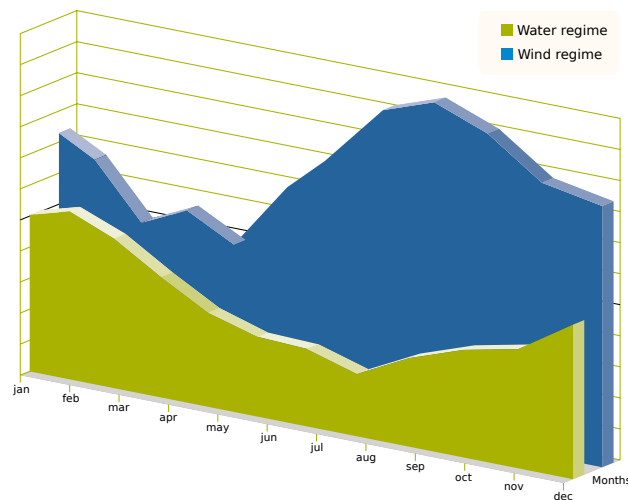
Source: ANEEL, 2005

1.2 Difficulties in Representing Wind Power Plants

With a growing share of energy covered by wind, system operators must consider how wind turbines affect the system stability during faults and maneuvers. To reach this goal, mathematical models capable of describing the behaviour of these machines are crucial.

Obtaining these models, on the other hand, is not an easy task, considering the great amount of wind turbines available, with different manufacturers, technologies, sizes and characteristics. Thus, a model that describes well a particular power plant will not necessarily work for others. Also, due to confidentiality, manufacturers provide little or no information about their wind turbine generators.

Particularly for wind power plants, an equivalent model is needed, since these facilities are usually widely spread and contain generators from different sizes and manufacturers. Besides, the distance to the substation is not the same for every generator in a wind power plants, as depicted in Figure 4. Hence, having one model for every wind turbine within a power plant would result in a mathematical problem with high complexity and computational cost (ERLICH et al., 2012).

Figure 4: Example of Wind Power Plant
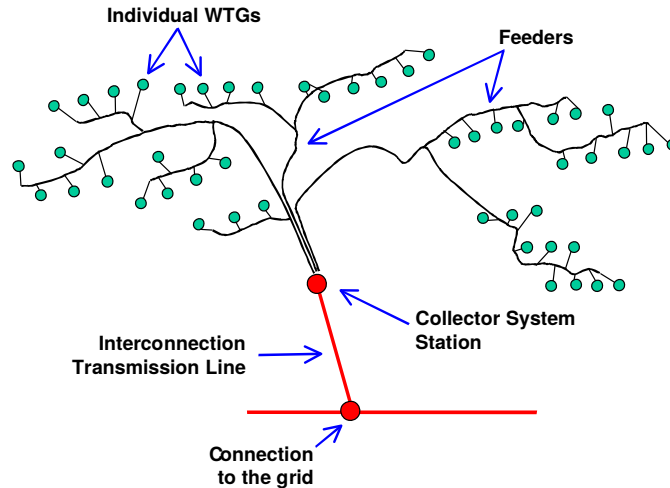
Source: Adapted from (MULJADI; ELLIS, 2008)

1.3 Research Goals

The main goal of this research is to estimate parameters of an equivalent model of a wind power plant used in transient stability studies. To achieve this goal, a hybrid algorithm for parameter estimation will be developed combining two methods: Mean-Variance Mapping Optimization, an population-based heuristic approach, and Trajectory

Sensitivity Method, a nonlinear approach. Also, as a secondary goal, a software, with graphical interface, for parameter estimation of nonlinear models will be developed. This research is a ongoing work of (CARI; ALBERTO; ERLICH, 2015), that focused on the parameter estimation using only Trajectory Sensitivity Method.

1.4 Work Organization

This section summarizes how the remainder of the text is organized. Chapter 2 will focus on the generic models for wind turbine generators and power plants and the selected mathematical model for parameter estimation purposes will be presented. The hybrid estimation process proposed and its methods will be subject to chapter 3, followed by the concept of the software under development on chapter 4. On chapter 5, the partial results obtained and the ongoing progress will be discussed.

2 MODELLING OF WIND TURBINE GENERATORS

Due to huge variety of wind turbine generators (WTG) and their different characteristics, modelling each machine of a wind power plant separately would be a long and exhaustive work. To address this problem, studies such as (MULJADI; ELLIS, 2008), (ELLIS et al., 2011), (COUNCIL, 2008) and (ASMINE et al., 2011), motivated specially by the Institute of Electrical and Electronics Engineers (IEEE) and the Western Electricity Coordinating Council (WECC), developed generic models able to predict the behaviour of entire wind power plants. Such models reduced the problem complexity, since they were composed of a single equivalent generator. A two-machine model is needed only in rare cases, such as when the wind power plant is composed of two or more types of wind turbines (ELLIS et al., 2011).

2.1 Generic Models of Wind Turbine Generators

The studies mentioned above have concluded that commercial wind turbine generators could be sorted into four basic types, according to their technology (ELLIS et al., 2011). These types are described in the following subsections.

2.1.1 Type-1: Squirrel Cage Induction Generator (SCIG)

The first type of wind turbine generator is composed of a Squirrel Cage Induction Generator (SCIG) connected to a wind turbine through a controlled gearbox, as displayed in Figure 5.

Figure 5: Representation of Type-1 Wind Turbine Generator
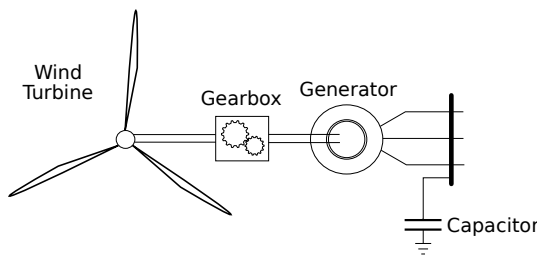
Due to its torque-speed characteristics, generators of this type operate at constant rotor speed, requiring robust controllers on gearbox and blade. Besides, as usual to any induction generator, the SCIG absorbs reactive power during operation. Thus, capacitors are often employed for power faction correction purposes. Moreover, type-1 generators limit aerodynamic power by varying the pitch angle of their blades, imposing great mechanical stress on blades, shafts and gears, demanding a robust mechanical design and preventing these generators to operate above certain wind speed (ELLIS et al., 2011).

2.1.2 Type-2: Wound Rotor Induction Generator (WRIG)

Similarly to Type-1 WTG, Type-2 Wind Turbine Generators are composed of an asynchronous machine connected to a wind turbine via gearbox, but, instead of SCIG, Wound Rotor Induction Generator (WRIG) are used to convert kinetic energy into electricity. The WRIG has access to its rotor windings, allowing to vary the rotor resistance. As a direct consequence, this machine can operate in different wind speeds by adjusting its torque-speed curve as needed (ELLIS et al., 2011). Therefore, Type-2 WTG have a WRIG with a variable resistance connected to its rotor terminals, as shown in Figure 6.

Figure 6: Representation of Type-2 Wind Turbine Generator
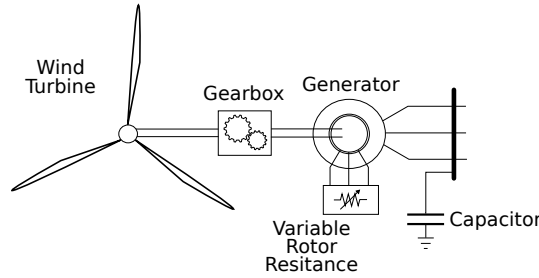
Thus, this type of generator has three speed control systems, with rotor resistance control responding to rapid changes in speed, gearbox control for medium variations and pitch control for slow changes. These control system work together to maintain power output constant and reduce mechanical stress on components. The effects on the torque-speed curve caused by different rotor resistances are shown in Figure 7.

Figure 7: Torque-speed curve
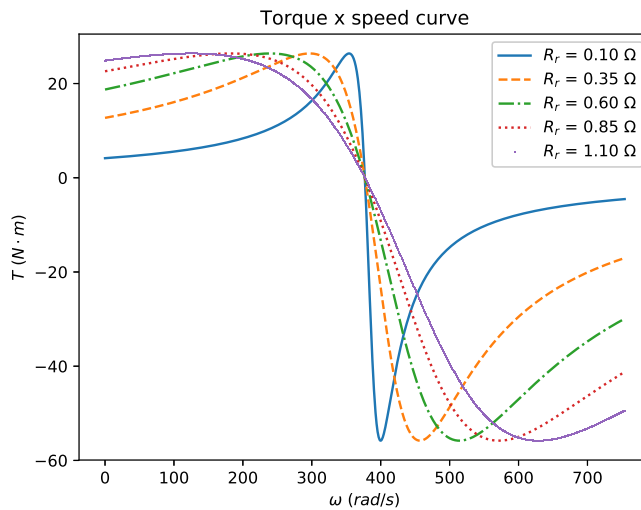
For a fixed power, increasing rotor resistance increases the speed needed on the shaft, allowing the wind turbine to operate above rated wind speed. However, the speed range is only $\pm 10\%$ of rated slip. Also, this machine still needs a reactive compensation circuit on its terminals (MULJADI et al., 2010).

2.1.3 Type-3: Doubly Fed Induction Generator (DFIG)

A Type-3 Wind Turbine Generator, often called Doubly Fed Induction Generator (DFIG), is also composed of a wound rotor machine connected to a wind turbine. But, instead of varying rotor resistance, a DFIG has its rotor supplied with AC voltage by a back-to-back frequency converter, as displayed in Figure 8.

Figure 8: Representation of Type-3 Wind Turbine Generator
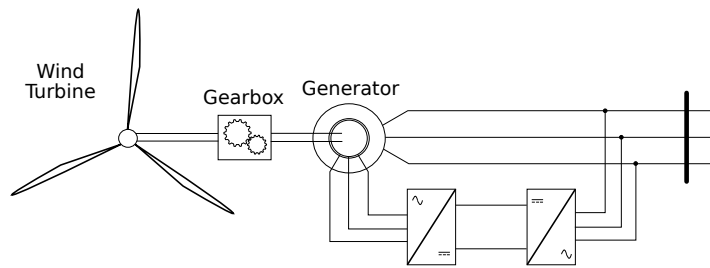

By varying the voltage frequency on the rotor circuit, the generator is able to supply power to the grid in a wider range of wind speed, reaching up to $\pm 30\%$ of rated slip. In addition, the converter can control both real and reactive power independently, ending the necessity of capacitors (MULJADI et al., 2010). Since approximately 30% of rated power flows through the rotor windings, power electronics components have lower specifications and do not have great impact on overall costs. On the other hand, these generators need regular maintenance due to slip rings, brushes and gearbox, preventing its use in offshore applications (YARAMASU et al., 2015).

2.1.4 Type-4: Full-Converter Generator

The last type of wind turbine generator, also called Full-Converter Generator, is composed of a electrical machine connected to the grid through a back-to-back frequency converter. The converter will operate converting the electrical frequency generated to standard, allowing this type of WTG to operate in a large range of wind speed (up to almost 100% of rated slip). Due to the converter operation, connection to the wind turbine can be made directly or via gearbox. Likewise, it allows the use of synchronous and asynchronous electrical machines as generator, with Permanent Magnet Synchronous Generator (PMSG), Electrical Excited Synchronous Generator (EESG) and SCIG being most common, because of cost and maintenance purposes. Similar to DFIG, full-converter generators are able to control real and reactive power injected into the grid. However,

since all power generated must flow through the power electronics, the overall cost of these generators is usually higher (YARAMASU et al., 2015). Figure 9 depicts a typical Type-4 Wind Turbine Generator.

Figure 9: Representation of Type-4 Wind Turbine Generator
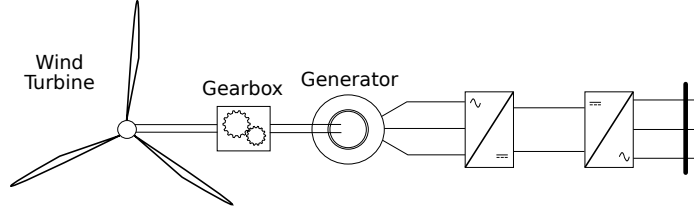
Figure 10 shows the evolution of share in installed capacity onshore for each generator type. The data shows how SCIG and WRIG lost space in the segment and how DFIG and Full-Converter Generators' participation rose, dominating the global market (MAGAGNA et al., 2017).

Figure 10: Share of installed capacity for each wind turbine generator type
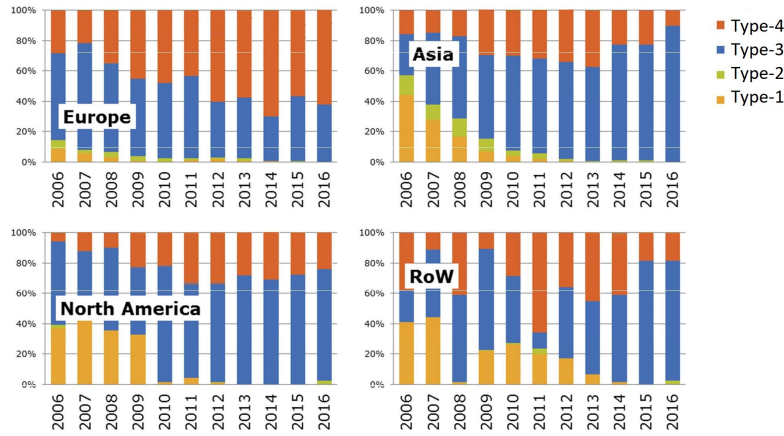
Source: Adapted from (MAGAGNA et al., 2017)

2.2 Model of Wind Turbine Generator Selected for Parameter Estimation

Many mathematical models were developed during the last years that are able to represent Wind Turbine Generators of all types. All those models have in common the fact that they are based on the generic models proposed by the studies made by WECC and IEEE and presented in the last chapter. The mathematical model selected for this work is presented in this section.

Initially proposed by (ERLICH et al., 2012), the mathematical model chosen is able to represent the dynamic behaviour of both Type-3 and -4 WTG's and can be used

to simulate entire wind power plants. Since the model is used on transient studies, it is assumed that wind speed and, consequently, mechanical power are constant during that interval. In this model, a Thevenin equivalent circuit is connected to grid with a controlled voltage source, as depicted in Figure 11.

Figure 11: Type-3 WTG model proposed by Erlich
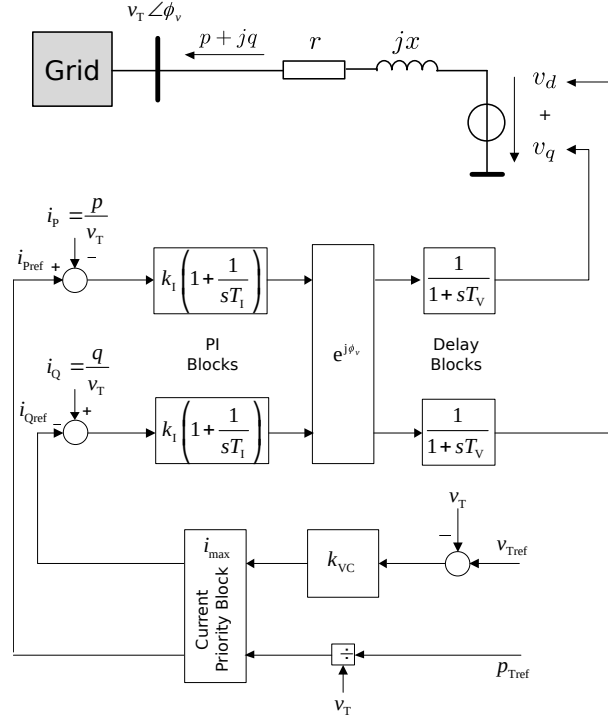
Source: Adapted from (ERLICH et al., 2012)

where v_T and ϕ_v correspond to the voltage magnitude and angle at substation bus, p and q are the active and reactive power produced by the generator, v_d and v_q stand for the generated voltage's direct and quadrature components, r and x correspond to the stator equivalent resistance and reactance, k_I and T_I are the PI block gain and time constant, T_V is the delay block time constant and k_{VC} is the voltage block gain.

Terminal voltage v_T is the variable of interest in this model, appearing as input to DFIG's control system. Active and reactive current are calculated using that input, according to equation (2.1).

$$\begin{cases} I_{Ac} = \frac{v_T}{p_{Tref}} \\ I_{Re} = k_{VC}(v_{Tref} - v_T) \end{cases} \tag{2.1}$$

The calculated currents feed a current priority block. This block analyses the current magnitude and terminal voltage level and decides whether power injection or voltage control will be prioritize. In summary, it checks if the generator's current is below

a maximum level i_{max} and, if it is not, the block verifies if terminal voltage is above a threshold value v^* to decide what will be prioritized. The following algorithm describes the current priority block operation.

if $\sqrt{I_{Ac}^2 + I_{Re}^2} \leq i_{max}$ then:
$$\begin{cases} i_{Pref} = I_{Ac} \\ i_{Qref} = I_{Re} \end{cases}$$

else:

    if $v_T \geq v^*$ then:
$$\begin{cases} i_{Pref} = min(i_{max}, I_{Ac}) \\ i_{Qref} = \sqrt{i_{max}^2 - i_{Pref}^2} \end{cases}$$

    else:
$$\begin{cases} i_{Qref} = min(i_{max}, I_{Re}) \\ i_{Pref} = \sqrt{i_{max}^2 - i_{Qref}^2} \end{cases}$$

The following PI blocks stand for the DFIG controllers (blade, gearbox, rotor-side and grid-side converters controllers) and their outputs follow the equations presented in (2.2).

$$\begin{cases} V_{PA} = k_I[(i_{Pref} - \frac{p}{v_T}) + \frac{1}{T_I} \int_0^t (i_{Pref} - \frac{p}{v_T}) dt] \\ \\ V_{QA} = k_I[(\frac{q}{v_T} - i_{Qref}) + \frac{1}{T_I} \int_0^t (\frac{q}{v_T} - i_{Qref}) dt] \end{cases} \tag{2.2}$$

Until here the controller operates on terminal voltage oriented coordinates, so a coordinate transformation block is needed to adequate to synchronous grid coordinates. This block operates according to equations (2.3).

$$\begin{cases} V_{PAS} = -V_{PA} cos(\theta_v) - V_{QA} sin(\theta_v) \\ V_{QAS} = V_{PA} sin(\theta_v) - V_{QA} cos(\theta_v) \end{cases} \tag{2.3}$$

Finally, two delay blocks supplying the voltage source (one for each component d and q) simulate the delay effects of the electrical machine and the back-to-back converter. Their effects are described by (2.4).

$$\begin{cases} \dot{v}_d = \frac{1}{T_V}(v_d - V_{PAS}) \\ \dot{v}_q = \frac{1}{T_V}(v_q - V_{QAS}) \end{cases} \tag{2.4}$$

The outputs of this model are real and reactive power produced by the WTG and their equations are shown below.

$$\begin{cases} P_e = \frac{r(v_{Td}v_d + v_{Tq}v_q - v_T^2) + x(v_{Tq}v_d - v_{Td}v_q)}{r^2 + x^2} \\ Q_e = \frac{x(v_{Td}v_d + v_{Tq}v_q - v_T^2) - r(v_{Tq}v_d - v_{Td}v_q)}{r^2 + x^2} \end{cases} \tag{2.5}$$

The summary of the model's equation is shown below:

$$\begin{cases} \dot{v}_d = \frac{1}{T_V}(v_d - V_{PAS}) \\ \dot{v}_q = \frac{1}{T_V}(v_q - V_{QAS}) \\ \\ P_e = \frac{r(v_{Td}v_d + v_{Tq}v_q - v_T^2) + x(v_{Tq}v_d - v_{Td}v_q)}{r^2 + x^2} \\ Q_e = \frac{x(v_{Td}v_d + v_{Tq}v_q - v_T^2) - r(v_{Tq}v_d - v_{Td}v_q)}{r^2 + x^2} \\ \\ V_{PAS} = -V_{PA}cos(\theta_v) - V_{QA}sin(\theta_v) \\ V_{QAS} = V_{PA}sin(\theta_v) - V_{QA}cos(\theta_v) \\ \\ V_{PA} = k_I[(i_{Pref} - \frac{p}{v_T}) + \frac{1}{T_I}\int_0^t(i_{Pref} - \frac{p}{v_T})dt] \\ V_{QA} = k_I[(\frac{q}{v_T} - i_{Qref}) + \frac{1}{T_I}\int_0^t(\frac{q}{v_T} - i_{Qref})dt] \end{cases} \tag{2.6}$$

if $\sqrt{I_{Ac}^2 + I_{Re}^2} \leq i_{max}$ then:
$$\begin{cases} i_{Pref} = I_{Ac} \\ i_{Qref} = I_{Re} \end{cases}$$
else:

if $v_T \geq v^*$ then:
$$\begin{cases} i_{Pref} = min(i_{max}, I_{Ac}) \\ i_{Qref} = \sqrt{i_{max}^2 - i_{Pref}^2} \end{cases}$$
else:
$$\begin{cases} i_{Qref} = min(i_{max}, I_{Re}) \\ i_{Pref} = \sqrt{i_{max}^2 - i_{Qref}^2} \end{cases}$$

$$\begin{cases} I_{Ac} = \frac{v_T}{p_{Tref}} \\ I_{Re} = k_{VC}(v_{Tref} - v_T) \end{cases}$$

Thus, this model can be interpreted as follows:

$$
\begin{cases}
\dot{x} = f(x, y, p, u) \\
y = g(x, p, u)
\end{cases}
\tag{2.7}
$$

where the state variables x, inputs u, outputs y and parameters p vectors are described by (2.8), (2.9), (2.10) and (2.11), respectively.

$$
x = [v_d, v_q]^T
\tag{2.8}
$$

$$
u = [v_T, \theta_v, P, Q]^T
\tag{2.9}
$$

$$
y = [P_e, Q_e]^T
\tag{2.10}
$$

$$
p = [r, x, k_I, T_I, T_V, k_{VC}]^T
\tag{2.11}
$$

The parameters presented in (2.11) are the subject of the estimation process presented on the next chapter. Those values define the behaviour of wind power plants during disturbances.

3 PARAMETER ESTIMATION PROCESS

Parameter estimation problems can be interpreted as optimization problems, where one must find the optimal values of parameters in order to reduce the error between real system and model outputs. During years, many methods were developed to address this problem, but two approaches have been largely employed to obtain its solution.

The first approach applies metaheuristics to obtain a sufficiently good solution. These methods are used in a variety of cases, ranging from biological to engineering problems, due to the fact that they are not developed for a specific type of problem. Metaheuristics employ a stochastic search to find (near-)optimal solutions inside a given region. However, those methods often take a great amount of time to converge to a solution (BLUM; ROLI, 2003). Examples of metaheuristics are Ant Colony Optimization, Differential Evolution, Particle Swarm Optimization and Genetic Algorithm. Applications of this approach in electrical power system cases can be found in (TODOROVSKI; RAJIČIĆ, 2006) and (YOSHIDA et al., 2000).

The second approach applies analytical methods to find the global optimum solution from equations derived from the problem. Thus, they are problem specific and must be adapted from one case to another. Analytical methods often converge in few iterations, reducing processing time, but they are sensitive to initial conditions. Some examples of analytical methods are Newton's Method, Kalman Filter, Unscented Kalman Filter, etc.

In this work is proposed to combine both approaches, reducing the effects of their disadvantages and improving overall convergence. Mean-Variance Mapping Optimization (MVMO) was the metaheuristic chosen for this problem, alongside Trajectory Sensitivity Method (TSM) as analytical method. Both methods will be discussed in the following sections.

The flowchart depicted in Figure 12 illustrates how the proposed method works. At first, a disturbance occurs, resulting in a dynamic response of the real system. The real system's outputs are compared to the model behaviour when the same disturbance is applied to it. The error $J(p)$ is evaluated through the Least-Squares Method, given by equation 3.1, where y_r and y stand for the real system and model outputs. While $J(p)$ is greater than a given tolerance tol_1, MVMO algorithm will search for a local solution. Afterwards, the error will eventually drop to a value lower than tol_1, and TSM will be used to refine the search to a optimal solution, with error level below tolerance tol_2.

$$J(p) = \frac{1}{2} \int_0^{T_0} (y_r(t) - y(t))^T (y_r(t) - y(t)) dt \tag{3.1}$$

Figure 12: Flowchart of estimation method
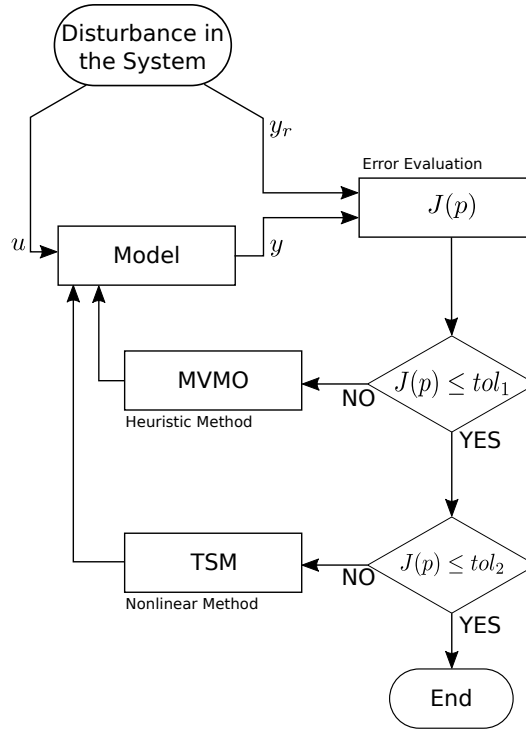
3.1 Mean-Variance Mapping Optimization Method

Presented in (ERLICH; VENAYAGAMOORTHY; WORAWAT, 2010), this population-based metaheuristic shares characteristics with other evolutionary algorithms, but differ from them on how to induce mutations on the offspring in order to diversify the population. By considering statistical data of population during mutation process, MVMO introduces a memory factor to it, enhancing search mechanism. Due this factor, MVMO performs better than similar metaheuristics when population size is relatively small (NAKAWIRO; ERLICH; RUEDA, 2011). The terms 'gene', 'individuals' and 'population' refer to 'parameter', 'parameter vector' and 'set of parameter vectors' in MVMO, for the sake of analogy.

Two other relevant concepts largely used on metaheuristics are exploration and exploitation. The first one refers to a broad search carried through the region of interest. On the other hand, exploitation means the search on a small neighbourhood close to the best solutions.

Before starting the parameter search process, a few settings must be done, such as population size, number of offspring, number of genes selected for mutation and selection method. Also, the search region is defined by setting the range within genes can vary. This constrains the parameters values within a feasible region, preventing divergence. The search region is later normalized for all genes, aiding the process. Termination criteria is

also set in this step. In this work, both number of generations and error will be used as stop criteria.

After that, a randomly-distributed population is generated, evaluated and sorted. Moreover, the mean and variance of every gene in each population are calculated. These values will later be used on the mutation process. The individual with lower error is selected as parent for a new generated individual. The offspring is then created following three steps common in evolutionary algorithms: gene selection, mutation and crossover. After creation, the offspring is introduced to the population and the worst individual is discarded, as depicted in Figure 13.

Figure 13: Exemplification of MVMO process
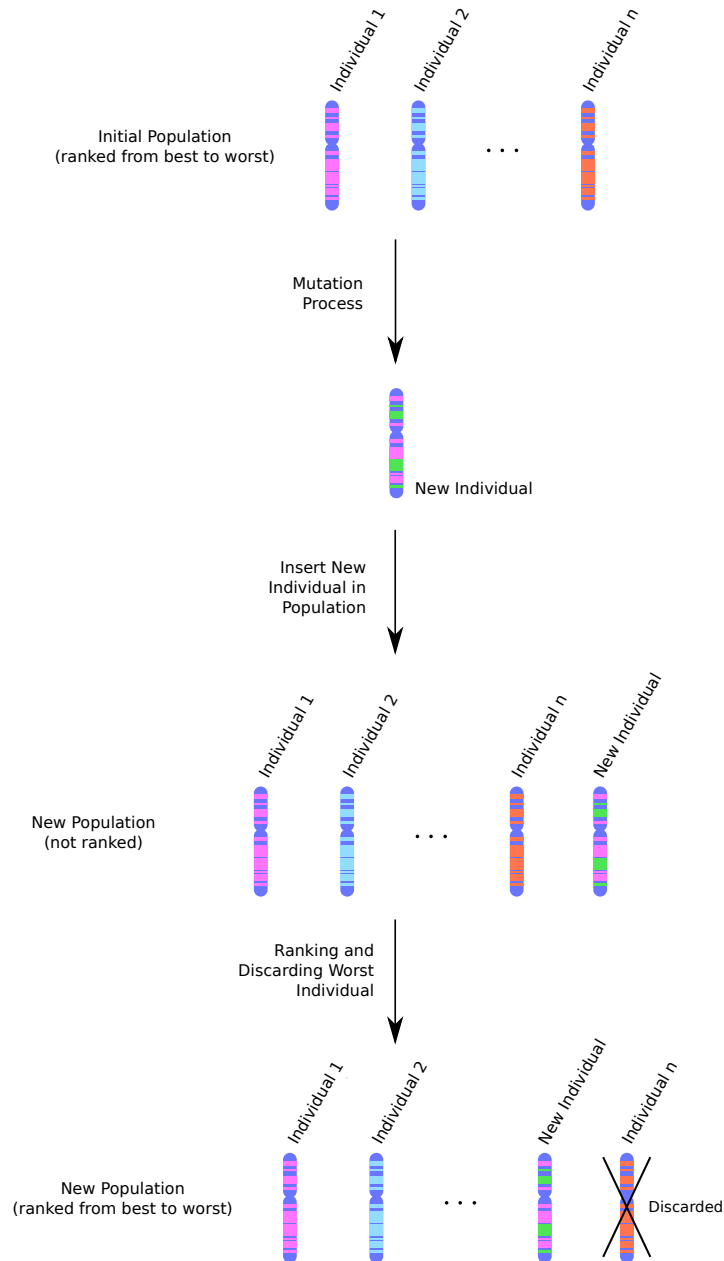
Gene selection can be done in many ways and even vary throughout the estimation process, with strategies' efficiency depending on the problem. However, three strategies are commonly used in this step. The first one is comprised of randomly selecting which genes will suffer mutation and which will be directly inherited from the parent. Gene selection can also be done by a moving window approach or even a combination of both strategies, with part of the genes selected at random and other through the window.

Mutation step takes place after gene selection. At first, each selected gene receives a random value x_i' between [0,1] that will be used as an input to a mapping function based on the mean and variance of each particular gene on the population. Variance v_i will directly influence on the shape factor given by (3.2), where f_s is the scaling factor responsible for focusing on exploration or exploitation. In the event of zero variance, the last non-null value of v_i is used.

$$s_i = -f_s ln(v_i) \tag{3.2}$$

Shape factor and mean value of genes of the population are used as inputs to a transformation function h, detailed in (3.3). The final value of the gene is obtained through the mapping function described by equation (3.4), where $h_x = h(u_i = x_i')$, $h_1 = h(u_i = 1)$ and $h_0 = h(u_i = 0)$. It is important to notice that the mapping function will always provide a result in the interval [0,1], not violating the normalization made at beginning.

$$h(\bar{x}_i, s_{i1}, s_{i2}, u_i) = \bar{x}_i(1 - e^{-u_i s_{i1}}) + (1 + \bar{x}_i)e^{-(1-u_i)s_{i2}} \tag{3.3}$$

$$x_i = h_x + (1 - h_1 + h_0)x_i' - h_0 \tag{3.4}$$

The resulting mapping function is depicted in Figure 14. The effects of different mean and shape factor values can be observed on Figure 15.

As shown in (3.3), two shape factors are used to evaluate the function. Different values of shape factors emphasizes the search below or above mean value. Thus, by controlling the values s_{i1} and s_{i2}, the method can prioritize exploration (global search) or exploitation (local search) on a given region. Figure 16 depicts how asymmetrical shape factors affect the mapping function.

The final step during offspring generation is crossover. During this phase, the mutated genes are united with the remaining genes inherited from parent, forming the new individual. This new individual is evaluated and included to the population if it is better than, at least, the population's worst individual. This process goes on until at least one stop criterion has been fulfilled.
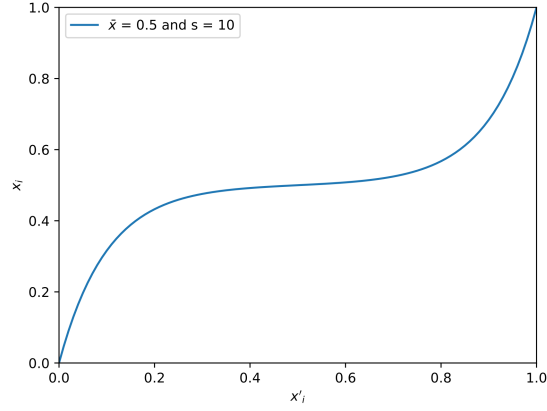
Figure 14: Example of MVMO mapping function

Figure 15: Effect of different mean and shape factor values on mapping function
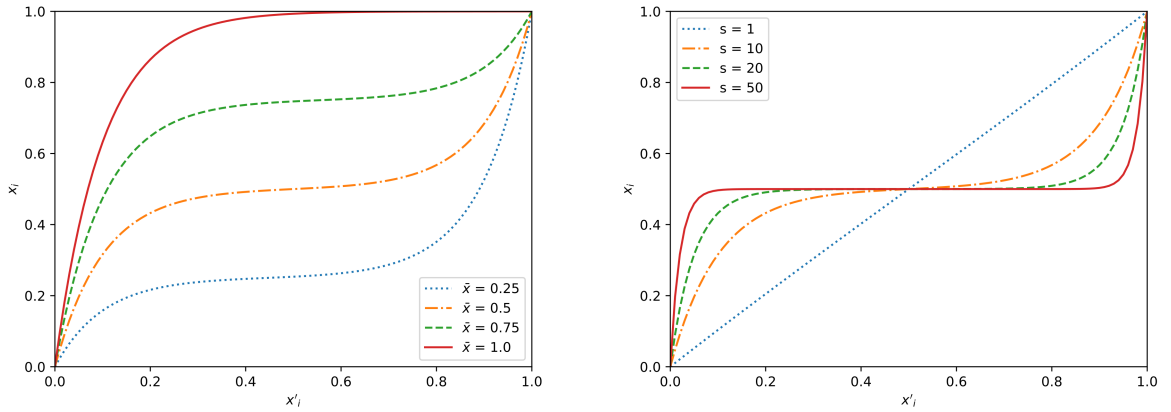
The main advantages of this method are low computational cost, good performance using small populations, constrained search region, preventing divergence, and the fact that it is non-specific. On the other hand, this method, as other metaheuristics, takes a great amount of time to converge when its error approaches zero.

3.2 Trajectory Sensitivity Method

Considering a nonlinear system described by (2.7), in order to minimize the error between model and real system, given by (3.1), one must discover a parameter vector p^* such as:

$$G(p^*) = \frac{\partial J(p^*)}{\partial p} = 0 \tag{3.5}$$

Figure 16: Comparison between symmetrical and asymmetrical shape factors
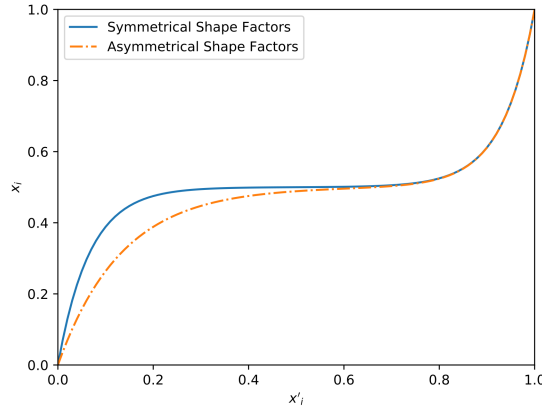
This derivative can be written as:

$$G(p) = -\int_0^{T_0} \left(\frac{dy}{dp}\right)^T (y_r - y)dt \tag{3.6}$$

Truncating the Taylor series for $G(p)$ on the first-order term results on (3.7). The matrix Γ is described in (3.8).

$$G(p^*) = G(p) + \Gamma(p)(p^* - p) \tag{3.7}$$

$$\Gamma(p) = \frac{\partial G(p)}{\partial p} \approx \int_0^{T_0} \left(\frac{dy}{dp}\right)^T \left(\frac{dy}{dp}\right) dt \tag{3.8}$$

By rearranging the terms on (3.7), the following equation is obtained. It describes how the parameters are updated after the nth iteration.

$$p^{n+1} = p^n + \Gamma^{-1}(p^n) \cdot G(p^n) \tag{3.9}$$

Obtaining the matrix of partial derivatives (also called trajectory sensitivities matrix) $\frac{\partial y}{\partial p}$, used in (3.6) and (3.8), analytically is an hard, when not impossible, task . In order to avoid problems when differentiating the system's equations, the definition of derivative, given by (3.10), can be used to approximate the values of the sensitivities.

$$\frac{df(x)}{dx} = \lim_{h \to 0} \frac{f(x+h) - f(x)}{h} \tag{3.10}$$

Consider two parameter vectors p and p^ϵ, where p^ϵ is obtained by adding a small perturbation ϵp_i to the $i - th$ element of p, as shown in (3.11).

$$p = \begin{bmatrix} p_1 \\ \vdots \\ p_i \\ \vdots \\ p_n \end{bmatrix} ; \quad p^\epsilon = \begin{bmatrix} p_1 \\ \vdots \\ p_i + \epsilon p_i \\ \vdots \\ p_n \end{bmatrix} \tag{3.11}$$

With ϵ sufficiently small, the partial derivative with respect to the parameter p_i can be approximated by the difference shown in equation (3.12). The value of $\epsilon = 0.1 \times 10^{-3}$ have shown great results for most cases. Using the approximation of the partial derivatives allows Trajectory Sensitivity method to be applied on both differentiable and non-differentiable systems (BENCHLUCH; CHOW, 1993), (CARI; ALBERTO; BRETAS, 2006).

$$\frac{\partial y(x, p, u)}{\partial p_i} \approx \frac{y(x, p^\epsilon, u) - y(x, p, u)}{\epsilon p_i} \tag{3.12}$$

The Trajectory Sensitivity Method has fast convergence characteristics and can applied directly to nonlinear problems, not requiring linearization. Also, by analyzing the sensitivities, the method provides information about parameters' identifiability. However, TSM is very sensitive to initial value of parameter chosen as starting point. Thus, if the initial values are too far from the real values, the method can either diverge or converge to wrong values. Besides, the information provided to the method must contain the effects of the parameters, otherwise they won't be observable (BENCHLUCH; CHOW, 1993).

By associating MVMO and TSM, the hybrid estimation approach proposed in this work combines most benefits of both methods whilst mitigating their disadvantages. The resulting method has smaller convergence time when compared to MVMO alone and is less sensitive to initial values of parameters than TSM.

4 SOFTWARE CONCEPT

In this chapter, the concept behind the software in development is presented. The entire software will be developed using Python, a powerful, simple and fast high-level programming language that has gained large space in various sectors of industry and academy. Its rise is due mainly to the enormous number of libraries and forums developed and maintained by the users. Some examples of libraries used in this project are *numpy* (for scientific computing), *matplotlib* (plotting library), *Tkinter* and *Qt* (Graphical User Interface toolkit). Python is also open-source, not requiring a paid software to code and most of its applications are free.

Although this project focus on using specific estimation methods and mathematical model for the DFIG problem, the software in development will not be specific to them. Instead, it will be generic and both model and method can be imported as packages. This will allow future users to use this application on different problems concerning parameter estimation. Also, comparison between method's performance and model's precision can be easily done with this software.

In order to improve the experience of users, a Graphical User Interface (GUI) will be developed. It will provide an simple environment for all users, so they won't need to go through the code to change any settings. Instead, the settings will be done at the beginning of the process and follow a predefined order.
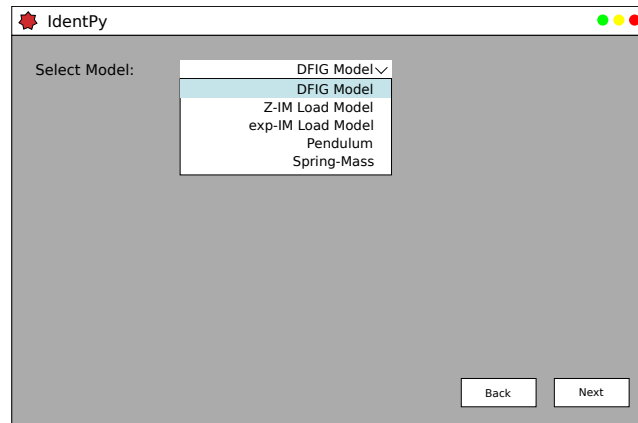
The starting window will display some information about the software and the parameter estimation process, as shown in Figure 17.

Figure 17: Representation of software starting window
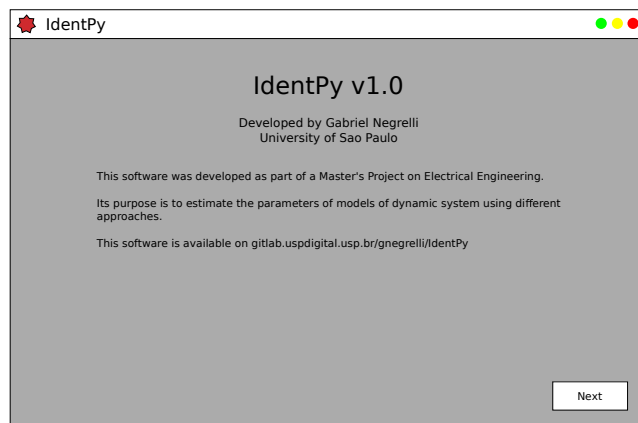
Next, the user will choose from a list which mathematical model will be employed, as depicted in Figure 18.

Figure 18: Representation of model selection window

After that, a list of identification methods will be presented and the user will be able to pick up to two methods, as displayed in Figure 19.

Figure 19: Representation of method selection window
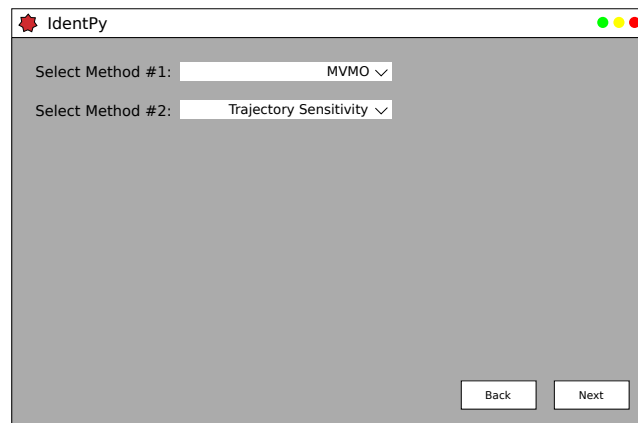
The settings of the chosen methods will done on the following windows and, finally, the user will enter the file containing the real system data and point out which data will be used as inputs and outputs. These steps are shown in Figures 20 and 21, respectively.

With all set, the estimation process will start and, at its end, a report will display the estimated parameters and the comparison between real system and model behaviours. The final view is represented in Figure 22

The order presented is not definitive and may change throughout the project if needed. However, all the steps discussed are core to the estimation process and cannot be discarded. Also, some other steps may be included in order to improve the software performance.
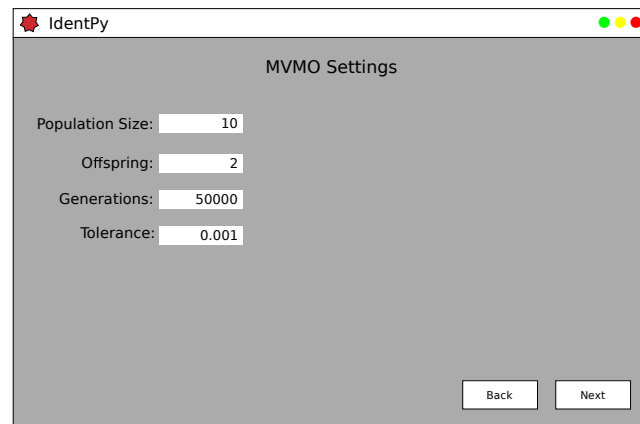
Figure 20: Representation of method setting window

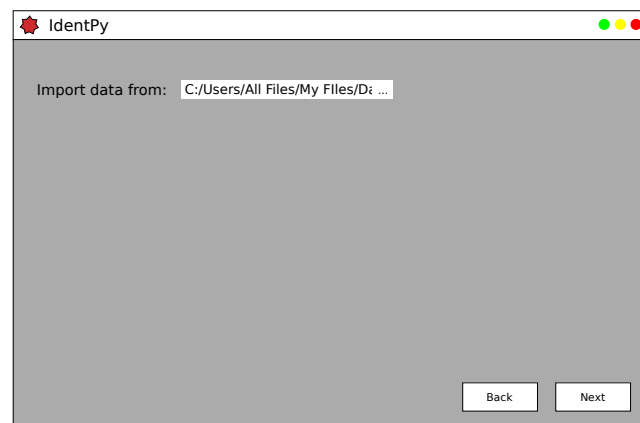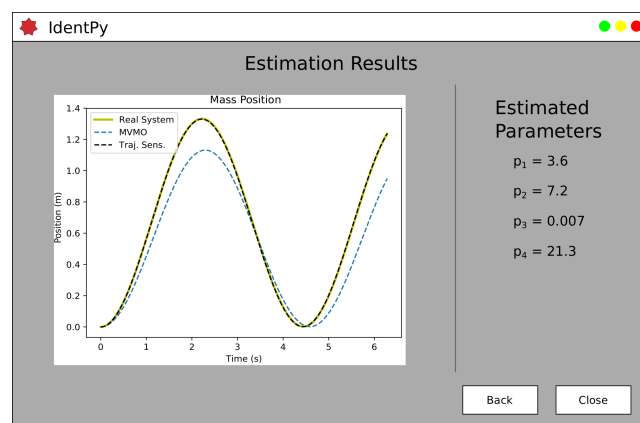
Figure 21: Representation of file selection window

Figure 22: Representation of report window

5 PARTIAL RESULTS

The expected result of this work is a estimation software for parameters of Type-3 WTG's mathematical model (2.6) in equation. To achieve this goal, the software will use the proposed hybrid estimation method of MVMO and TSM.

The measurements will be obtained from a small power system simulated on specific software, such as DIgSILENT or MATLAB. At first, the model proposed in (ERLICH et al., 2012) will be employed, but it can be further changed if needed. Also, other estimation methods, such as Particle Swarm Optimization, Differential Evolution or Kalman Filters, may be implemented for comparison purposes.

The hybrid approach for parameters estimation presented in this work is already implemented and have shown great results for different models. For learning and testing purposes, the proposed approach was used to estimate parameters of simpler systems, such as the spring-mass system, for testing purposes, but also in complex applications, such as load models. The results obtained from those systems are presented in the following subsections.

5.1 Application of Hybrid Method on Spring-Mass System

The spring-mass system is a simple physical model often used as example of dynamic systems. It is composed of an object of mass m connected to a fixed point in space by a spring of stiffness constant k. When disturbed by an external force u, the object oscillates and its movement is described by (5.1), x is the position of the object while x_1 and x_2 correspond to its speed and acceleration, respectively. The system output, parameter vector, input and initial conditions are presented on (5.2), (5.3), (5.4) and (5.5), respectively.

$$\begin{bmatrix} \dot{x_1} \\ \dot{x_2} \end{bmatrix} = \begin{bmatrix} 0 & 1 \\ \frac{k}{m} & 0 \end{bmatrix} \cdot \begin{bmatrix} x_1 \\ x_2 \end{bmatrix} - \begin{bmatrix} 0 \\ \frac{1}{m} \end{bmatrix} \cdot u \tag{5.1}$$

$$y = \begin{bmatrix} x_1, x_2 \end{bmatrix}^T \tag{5.2}$$

$$p = \begin{bmatrix} m, k \end{bmatrix}^T \tag{5.3}$$

$$u = 1 \tag{5.4}$$

$$\begin{cases} x_1(0) = 0 \\ x_2(0) = 0 \end{cases} \tag{5.5}$$

The behaviour of the real system was obtained through simulation with parameters set at $m = 3\ kg$ and $k = 6\ N/m$. Three different estimation process were executed: TSM, MVMO and the hybrid approach of MVMO and TSM combined. The tolerance for all three estimations was set at $tol = 0.1$.

5.1.1 Trajectory Sensitivity Results

It took only 7 iterations (7 seconds on a PC) for Trajectory Sensitivity Method to estimate the parameters when the initial values were $m_0 = 7\ kg$ and $k_0 = 7\ N/m$. This shows how fast this method is, as long as the initial values are in the neighbourhood of the real parameters. Figure 23 shows the error evolution during estimation suing TSM.

Figure 23: Error evolution of TSM with $m_0 = 7\ kg$ and $k_0 = 7\ N/m$
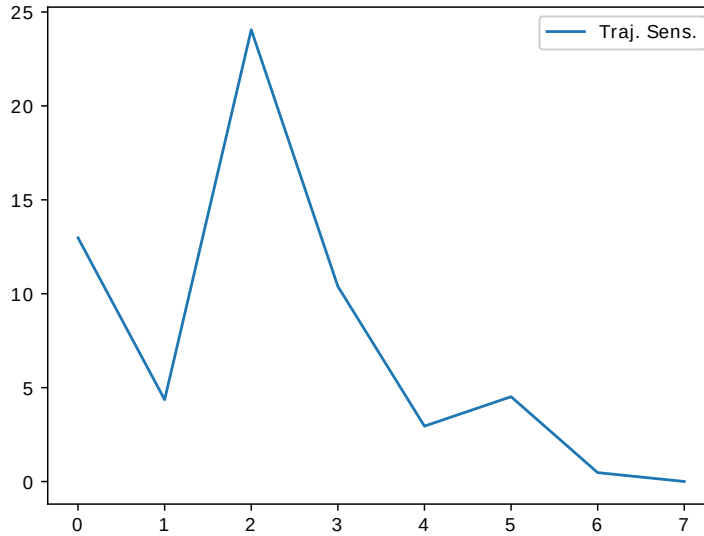
However, the convergence region [1] of TSM is extremely limited, diverging from initial points far enough from the real values. The convergence region for the real values was obtained in (FARIAS; CARI, 2016) and is shown in Figure 24. For comparison, the MVMO and the hybrid approach converge for the entire search region displayed on the graph.

To illustrate the importance of good initial values, the parameters were reestimated using TSM, but now the initial values were set to be $m_0 = 8\ kg$ and $k_0 = 10\ N/m$. Notice that these values are not too far from the ones used in the previous estimation. The results,

---

[1] Convergence region is a region in parameter space where, if the initial guess for parameter values is inside it, the convergence to true values is guaranteed.

Figure 24: Convergence region of Trajectory Sensitivity Method
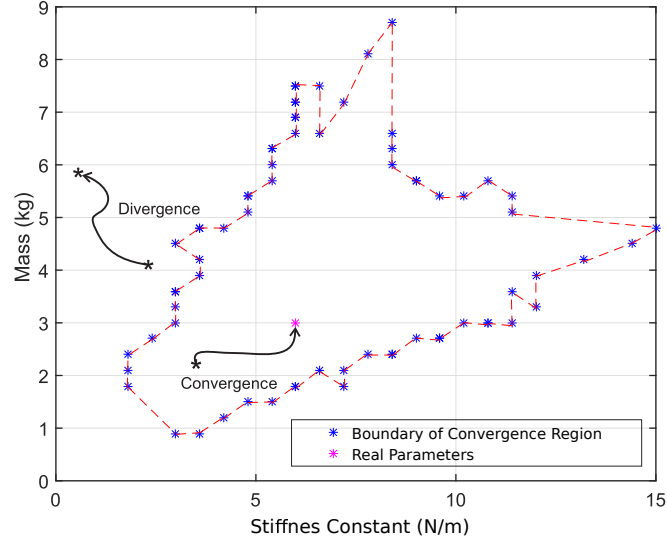
Source: Adapted from (FARIAS; CARI, 2016)

on the other hand, were extremely different. The method was not able to lower the error below 16.4 and the parameters found were $m_f = 2.7\ kg$ and $k_f = 118.6\ N/m$. The error evolution for this estimation is depict in Figure 25.

Figure 25: Error evolution of TSM with $m_0 = 8\ kg$ and $k_0 = 10\ N/m$
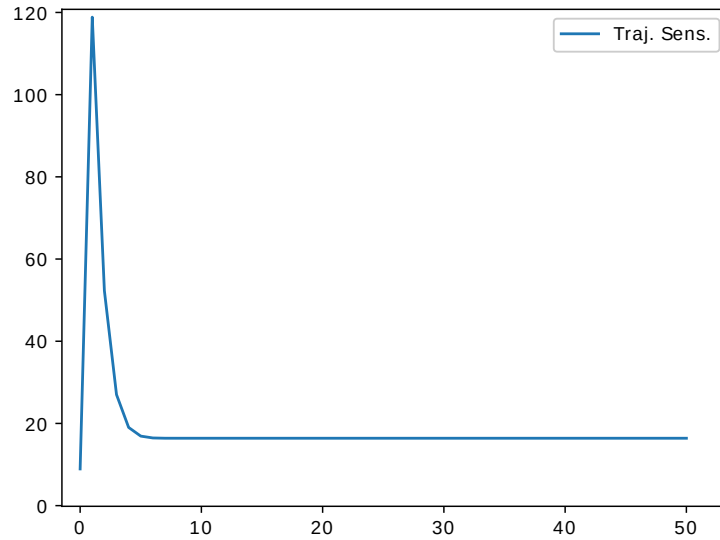
5.1.2 MVMO Results

To use MVMO, a search region in parameter space must be defined. Therefore, the parameters' boundaries was defined as $0 \leq m \leq 9$ and $0 \leq k \leq 15$. The population size was ate 5 individuals and after every generation 1 new individual was created. The heuristic

method converged after almost 10000 generations, as depicted in Figure 26. This figure also shows how MVMO rapidly reduces error of estimation, but as the values approach the neighbourhood of the real values, it slows down.

Figure 26: Error evolution of MVMO
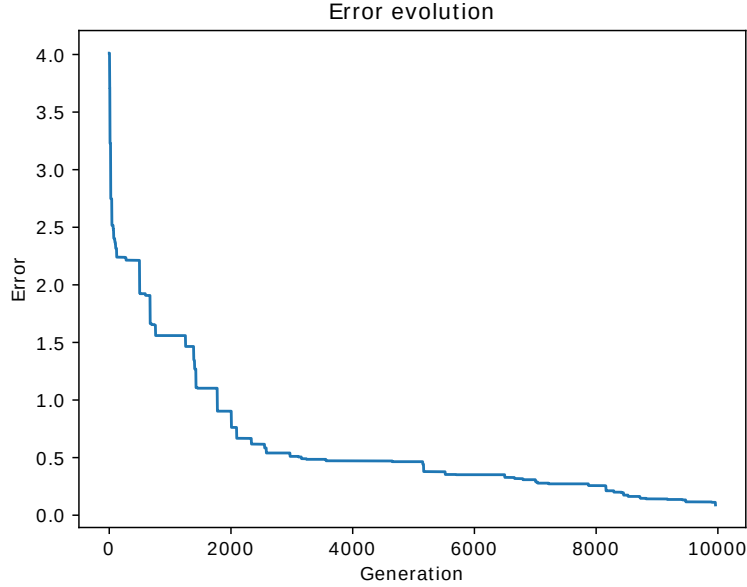
5.1.3 Hybrid Approach Results

By combining both methods, the hybrid approach benefits from the quick error reduction provided by MVMO and the fast convergence from TSM when inside convergence region. The error evolution obtained from this approach is depicted in Figure 27. The tolerance for this approach were set at $tol_1 = 1.5$ and $tol_2 = 0.1$.

When compared to each method, the hybrid approach converges faster than MVMO but slower than TSM, as shown in Table 1. Although all methods converged to parameter values that resulted in an error level below the tolerance, TSM and the Hybrid approach provided better results than MVMO with final error close to 2.0×10^{-3}.

Table 1: Comparison of approaches

Approach	Time	Final Error
TSM	$7\ s$	2.76×10^{-3}
MVMO	$24\ min$	89.33×10^{-3}
Hybrid	$10\ min$	1.54×10^{-3}

5.2 Application of Hybrid Method on Linearized Z-IM Load Model

The hybrid approach was also employed on parameter estimation of Z-IM Load Model. This model is able to predict the behaviour of electrical loads during faults in the

Figure 27: Results of hybrid approach for spring-mass system
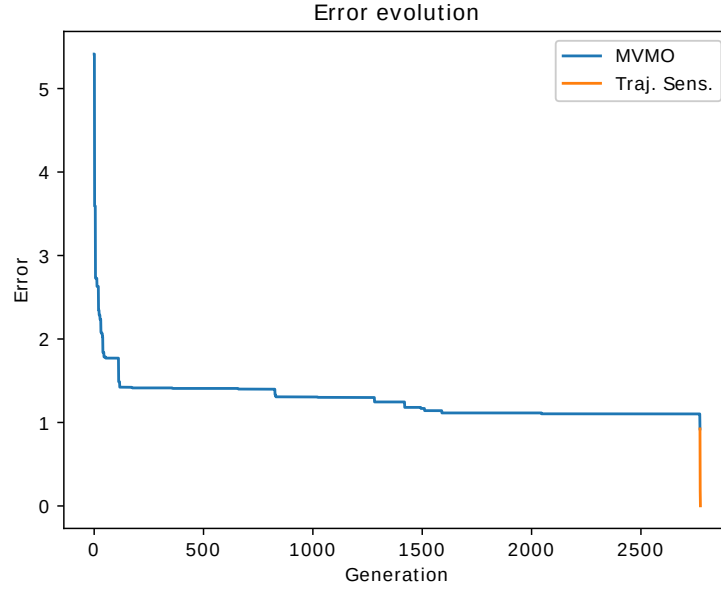
grid. The Z-IM Load Model is composed of a impedance in parallel with a third-order induction motor (IM), as shown in Figure 28. According to (CHOI et al., 2006), this model results in low error levels for both active and reactive power, alongside having a smaller parameter vector when compared with other models. It is described by the following equations:
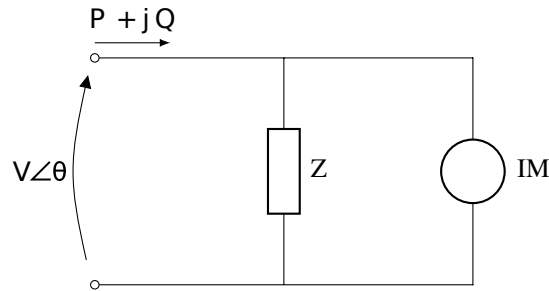
Figure 28: Schematic of Z-IM Load Model.

$$
\begin{cases}
\Delta \dot{E'} = \frac{-1}{T_o X'}[X\Delta E' + (X - X')V_0 \sin \delta_0 \Delta \delta] + \frac{(X-X')\cos \delta_0}{T_0 X'}\Delta V \\[2em]
\Delta \dot{\delta} = \frac{(X-X')V_0}{T_0 X' E_0'} \cdot \left(\frac{\sin \delta_0 \Delta E'}{E_0'} - \cos \delta_0 \Delta \delta \right) + \Delta \omega - \frac{(X-X')\sin \delta_0}{T_o X' E_0'}\Delta V \\[2em]
\Delta \dot{\omega} = \frac{-V_0}{MX'}(\sin \delta_0 \Delta E' + E_0' \cos \delta_0 \Delta \delta) - \frac{E_0' \sin \delta_0}{MX'}\Delta V
\end{cases}
\quad (5.6)
$$

$$\begin{cases} \Delta P = \frac{-V_0}{X'}\left(\sin\delta_0 \Delta E' + E_0' \cos\delta_0 \Delta\delta\right) + \left(2G_s V_0 - \frac{E_0' \sin\delta_0}{X'}\right)\Delta V \\ \\ \Delta Q = \frac{-V_0}{X'}\left(\cos\delta_0 \Delta E' + E_0' \sin\delta_0 \Delta\delta\right) + \left(2B_s V_0 + \frac{2V_0 - E_0' \cos\delta_0}{X'}\right)\Delta V \end{cases} \tag{5.7}$$

$$\begin{cases} X = X_s + X_m \\ X' = X_s + \frac{X_m X_r}{X_m + X_s} \\ T_o = \frac{X_r + X_m}{\omega_s R_r} \end{cases} \tag{5.8}$$

where the terms $\Delta E'$ and $\Delta\delta$ represent the variation on voltage magnitude and angle at the motor terminals, $\Delta\omega$ is the variation on stator speed, in rad/s. X_m, X_s and X_r are the magnetizing, stator and rotor reactances, respectively, R_r stands for the rotor resistance, ω_s is the synchronous speed, T_o represents the open-circuit transient time constant, M is the motor inertia and V_0 is the voltage on the load terminals before the disturbance. The state, output, input and parameter vectors are presented in (5.9), (5.10), (5.11) and (5.12), respectively.

$$x = [\Delta E', \Delta\delta, \Delta\omega]^T \tag{5.9}$$

$$y = [\Delta P, \Delta Q]^T \tag{5.10}$$

$$u = [\Delta V] \tag{5.11}$$

$$p = [X, X', T_0, M, G_s, B_s, E_0', \delta_0]^T \tag{5.12}$$

The Z-IM load model is much more complex than the spring-mass system, with 9 parameters to be estimated. The hybrid approach proposed was able to estimate the parameters of this system and the comparison between real and modeled behaviour with the parameters obtained can be seen in the Figure 29.

The application of the hybrid approach on Linearized Z-IM Load Model is subject of a paper presented by the author on the 2019 IEEE Canadian Conference on Electrical and Computer Engineering entitled "*Load Model Identification Through a Hybrid Approach*".

5.3 Ongoing Progress

With the methods already implemented and tested, the focus is now on the DFIG model. The model has presented some results, but it is not as accurate as expected,

Figure 29: Result of parameter estimation for Z-IM Load Model
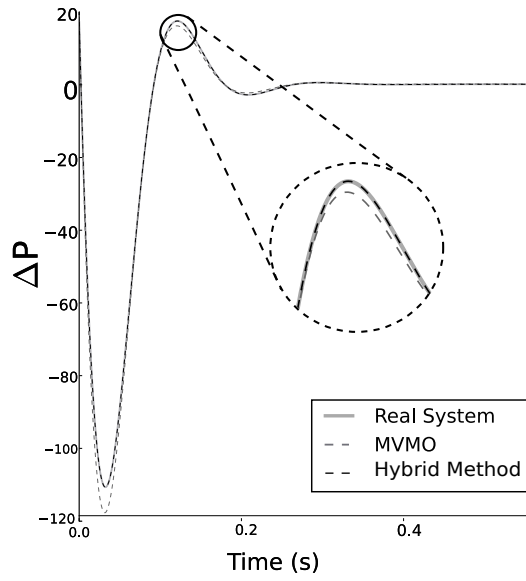
Source: (GOMES et al., 2019)

requiring some studies about this topic. The implementation of other WTG models for comparison is also under study.

The simulation of wind turbine generators and power plants on specific software will be carried out on the next months. The GUI is under development and already has some features implemented using Python's library *Tkinter*. A proposal to also develop features using *Qt*, a different GUI tool package, is currently under consideration.

The summary of this work's next steps is presented in Table 2.

Table 2: Summary of next steps

Data Acquisition	WTG Modelling	Estimation Method	GUI
Synthetic data will be obtained via simulation.	Model implemented with bad results. Improvements currently under study.	Method implemented and tested. Improvements under study.	Concept defined. Some windows have already been implemented.

BIBLIOGRAPHY

ABEEOLICA. **Annual Wind Energy Report**. Sao Paulo, 2018.

AMARANTE, O. A. C. do et al. **Atlas do Potencial Eólico Brasileiro**. Brasilia, 2001.

ANEEL. **Atlas de Energia Elétrica do Brasil**. Brasilia, 2005. Disponível em: <http://www.aneel.gov.br/livros/-/asset{_}publisher/eZ674TKh9oF0/content/atlas-de-energia-eletrica-do-brasil/656>.

ASMINE, M. et al. Model Validation for Wind Turbine Generator Models. **Power Systems, IEEE Transactions on**, v. 26, n. 3, p. 1769–1782, 2011. ISSN 0885-8950.

BENCHLUCH, S. M.; CHOW, J. H. A Trajectory Sensitivity Method for the Identification of Nonlinear Excitation System Models. **IEEE Transactions on Energy Conversion**, v. 8, n. 2, p. 159–164, jun 1993. ISSN 15580059. Disponível em: <http://ieeexplore.ieee.org/document/222699/>.

BLUM, C.; ROLI, A. Metaheuristics in Combinatorial Optimization: Overview and Conceptual Comparison. **ACM Computing Surveys**, v. 35, n. 3, p. 268–308, sep 2003. ISSN 0360-0300. Disponível em: <http://portal.acm.org/citation.cfm?doid=937503.937505>.

CARI, E. P.; ALBERTO, L. F.; BRETAS, N. G. A methodology for parameter estimation of synchronous generators based on trajectory sensitivity and synchronization technique. In: **2006 IEEE Power Engineering Society General Meeting, PES**. IEEE, 2006. p. 6 pp. ISBN 1424404932. Disponível em: <http://ieeexplore.ieee.org/document/1709492/>.

CARI, E. P. T.; ALBERTO, L. F. C.; ERLICH, I. Assessment of model parameters to identify an equivalent wind power plant. In: **2015 IEEE Eindhoven PowerTech, PowerTech 2015**. IEEE, 2015. p. 1–5. ISBN 9781479976935. Disponível em: <http://ieeexplore.ieee.org/document/7232472/>.

CHOI, B. K. et al. Measurement-based dynamic load models: Derivation, comparison, and validation. **IEEE Transactions on Power Systems**, 2006. ISSN 08858950.

COUNCIL, W. E. C. Wecc wind power plant power flow modeling guide. **WECC Wind Generator Modeling Group, Tech. Rep**, 2008.

ELLIS, A. et al. Generic models for simulation of wind power plants in bulk system planning studies. **IEEE Power and Energy Society General Meeting**, p. 1–8, 2011. ISSN 19449925.

EPE. **Anuário Estatístico de Energia Elétrica 2018 no ano base de 2017**. Rio de Janeiro, 2018. 249 p. Disponível em: <http://www.epe.gov.br/sites-pt/publicacoes-dados-abertos/publicacoes/PublicacoesArquivos/publicacao-160/topico-168/Anuario2018vf.pdf>.

ERLICH, I. et al. Determination of Dynamic Wind Farm Equivalents using Heuristic Optimization. **Power and Energy Society General Meeting, IEEE**, p. 1–8, 2012.

ERLICH, I.; VENAYAGAMOORTHY, G. K.; WORAWAT, N. A Mean-Variance Optimization algorithm. **2010 IEEE World Congress on Computational Intelligence, WCCI 2010 - 2010 IEEE Congress on Evolutionary Computation, CEC 2010**, n. February, p. 1–6, 2010.

European Commission. **A strategy for smart, sustainable and inclusive growth**. Brussels, 2010. 1–37 p. Disponível em: <https://www.eea.europa.eu/policy-documents/com-2010-2020-europe-2020>.

FARIAS, E. R. C.; CARI, E. P. T. **Parameter estimation of an induction generator based on the sensitivity trajectory method**. 2016. Monography, USP (University of Sao Paulo), Sao Carlos, Brazil.

Federative Republic of Brazil. **Lei 10438/2002**. Brasilia: [s.n.], 2002. 1–21 p. Disponível em: <http://www.planalto.gov.br/ccivil{_}03/leis/2002/L10438.htmhttp://www.planalto.gov.br/ccivil{_}03/LEIS/2002/L104>.

GOMES, G. J. N. et al. Load Model Identification Through a Hybrid Approach. In: **2019 IEEE Canadian Conference on Electrical and Computer Engineering**. Edmonton: [s.n.], 2019.

MAGAGNA, D. et al. **Supply chain of renewable energy technologies in Europe: An analysis for wind, geothermal and ocean energy**. [S.l.], 2017. Disponível em: <https://ec.europa.eu/jrc/en/publication/eur-scientific-and-technical-research-reports/supply-chain-renewable-energy-technologies-europe-analysis-wind-geothermal-and-ocean-energy>.

MULJADI, E.; ELLIS, A. Validation of wind power plant models. **IEEE Power and Energy Society 2008 General Meeting: Conversion and Delivery of Electrical Energy in the 21st Century, PES**, p. 1–7, 2008. ISSN 1932-5517.

MULJADI, E. et al. Short circuit current contribution for different wind turbine generator types. In: **IEEE PES General Meeting, PES 2010**. IEEE, 2010. p. 1–8. ISBN 9781424483570. Disponível em: <http://ieeexplore.ieee.org/document/5589677/>.

NAKAWIRO, W.; ERLICH, I.; RUEDA, J. L. A novel optimization algorithm for optimal reactive power dispatch: A comparative study. **2011 4th International Conference on Electric Utility Deregulation and Restructuring and Power Technologies (DRPT)**, n. 1, p. 1555–1561, 2011. ISSN 0278-0046. Disponível em: <http://ieeexplore.ieee.org/document/5994144/>.

TODOROVSKI, M.; RAJIČIĆ, D. An initialization procedure in solving optimal power flow by genetic algorithm. **IEEE Transactions on Power Systems**, v. 21, n. 2, p. 480–487, 2006. ISSN 08858950.

Wind Europe. Wind energy in Europe in 2018: Trends and statistics. **Wind Europe. (2019). Wind energy in Europe in 2018: Trends and statistics.**, 2019. ISSN 0309524X.

XIONG, L. et al. Stability Enhancement of Power Systems With High DFIG-Wind Turbine Penetration via Virtual Inertia Planning. **IEEE Transactions on Power Systems**, v. 34, n. 2, p. 1352–1361, mar 2019. ISSN 0885-8950. Disponível em: <https://ieeexplore.ieee.org/document/8463592/>.

YARAMASU, V. et al. High-power wind energy conversion systems: State-of-the-art and emerging technologies. **Proceedings of the IEEE**, v. 103, n. 5, p. 740–788, may 2015. ISSN 00189219. Disponível em: <http://ieeexplore.ieee.org/document/7109820/>.

YOSHIDA, H. et al. A Particle swarm optimization for reactive power and voltage control considering voltage security assessment. **IEEE Transactions on Power Systems**, 2000. ISSN 08858950.